

Transport in Thin Gravity-driven Flow over a Curved Substrate

Jean-Luc Thiffeault* and Khalid Kamhawi

Department of Mathematics, Imperial College London, SW7 2AZ, United Kingdom

(Dated: 31 July 2006)

We consider steady gravity-driven flow of a thin layer of viscous fluid over a curved substrate. The substrate has topographical variations ('bumps') on a large scale compared to the layer thickness. Using lubrication theory, we find the velocity field in generalized curvilinear coordinates. We correct the velocity field so as to satisfy kinematic constraints, which is essential to avoid particles escaping the fluid when computing their trajectories. We then investigate the particle transport properties of flows over substrates with translational symmetry, where chaotic motion is precluded. The existence of trapped and untrapped trajectories leads to complicated transport properties even for this simple case. For more general substrate shapes, the trajectories chaotically jump between trapped and untrapped motions.

PACS numbers: 47.85.mf; 47.15.gm; 47.52.+j

Keywords: thin flows; lubrication theory; chaotic advection; particle transport

I. INTRODUCTION

It is often the case in applications that viscous fluid flows in a thin layer at low Reynolds number, which allows lubrication (or long-scale, also long-wave) theory to be used.¹ The resulting decoupling between the long-scale and the 'thin' direction greatly simplifies the mathematical solution of the flow. There is essentially only one equation to be solved, for the thickness of the fluid as a function of position. This equation arises from mass conservation appropriately averaged over the thin coordinate. The velocity is then deduced from the thickness.

The mass-conservation equation to be solved involves only the long-scale coordinates. The third coordinate is 'slaved' to the horizontal ones by the effect of viscosity. In that sense one usually thinks of thin-layer flows as 'two-dimensional,' in the sense that vertical variations (*i.e.*, in the thin direction) exist but are subsumed in the theory and that the vertical velocity field is small. However, if one is interested in the transport properties of such flows, any amount of vertical variation is crucial. We will show here that even small variations can lead to chaotic behavior of particle trajectories, known as chaotic advection,²⁻⁴ greatly enhancing the transport properties of the flow. Indeed, if the flow were truly two-dimensional and steady, chaotic transport would be impossible since two-dimensional autonomous dynamical systems cannot exhibit chaos.⁵

As far as we know, the transport properties of thin-layer flows have not been studied, beyond plotting streamlines in two-dimensional cases, probably because they were assumed

*Electronic address: jeanluc@imperial.ac.uk

too simple to be important. But understanding these properties could be important if, for instance, a compositionally-uniform coating is required in an industrial application. A related area that has received much attention lately is chaotic advection in microchannels.⁶ There periodic grooved patterns at the bottom of the channel cause swirl in the flow that leads to chaos. Here we study a different regime where the bottom substrate has larger topographical variations, the fluid is thinner, and the sidewalls are less important.

We will show here that the shape of the curved substrate is crucial. Though we investigate this for the case of steady gravity-driven flow with a free surface, the conclusions reached should qualitatively apply to different thin-flow situations such as those driven by surface tension gradients. Constant surface tension is included in the derivation, but left out of most of the examples since it does not affect the qualitative results.

There are several derivations of models of thin fluid flow over curved substrates in the literature.^{7–12} Our approach follows that of Roy *et al.*⁸ (hereafter RRS), in that the vertical (thin-direction) coordinate is orthogonal to the long-scale coordinates, but differs in that the long-scale coordinates are not necessarily orthogonal to each other. This is because even though orthogonal coordinates can always be found,¹³ doing so for a general substrate (other than planes, cylinders, and spheres) requires solving differential equations numerically. Working in generalized coordinates is not much more complicated if differential-geometric notation is used,^{14–16} and allows a simple parametrization of the substrate in terms of a height function.

Another motivation for re-deriving the model of RRS⁸ is that we need to include correction terms to the mass-conservation equation and vertical velocity to ensure that the kinematic boundary condition at the free surface is satisfied exactly, up to numerical accuracy. In the RRS model, the kinematic boundary condition is satisfied to second order in the thickness. This is fine for most applications, but for particle advection it is catastrophic: in numerical simulations, individual particles will gleefully escape the top surface if they come anywhere near it, since even a second-order error is enough to give a small component of the velocity field normal to the surface. Rather than remedy this in some ad-hoc manner (by reflecting the particles back in, for instance), we instead include some judiciously-chosen second-order terms that guarantee that the kinematic boundary condition at the top surface is satisfied.

The outline of the paper is as follows. Sections II–IV comprise the derivation of the model equations. At each stage, we carefully record where the thinness of the layer comes in as an approximation. Since we will be working with substrates of complicated shapes, the first part of our paper (Section II) is devoted to establishing a convenient coordinate system for our problem. Then we tackle mass conservation in those coordinates in Section III. Section IV introduces the dynamical equations of motion for Stokes flow. In that section we also rescale the variables (Section IV A) and solve for the velocity field (Section IV B) to first order in the thickness. This gives the mass flux vector, whose divergence must vanish for steady flow. We include second-order terms to the mass flux to impose the kinematic boundary condition at the free surface, which is essential for particle advection as discussed above.

In Section V we discuss solutions of the governing PDE for the fluid thickness. The simplest type of solution involves substrates with a translational symmetry, for which the steady flow can be found analytically at leading order. However, solving for the flow at first order, or for substrates without such a symmetry, we must resort to numerical solutions.

Section VI is concerned with fluid particle advection and is the central results section of the paper. We examine the variety of particle trajectories by making Poincaré surfaces

of section, for increasingly complicated substrates. As expected, the transport properties also become more complicated, exhibiting a range of behavior from trapped to chaotic trajectories. We offer some concluding remarks in Section VII.

II. COORDINATE SYSTEM

A. Separating the Thin Direction

In our problem, fluid motion occurs over a curved substrate of arbitrary shape. The direction normal to the substrate is special in that it defines the direction in which the fluid layer is assumed ‘thin.’ Hence, it is convenient to locate a point \mathbf{r} in the fluid as

$$\mathbf{r}(x^1, x^2, y) = \mathbf{X}(x^1, x^2) + y \hat{\mathbf{e}}_3(x^1, x^2) \quad (\text{II.1})$$

where $\mathbf{X}(x^1, x^2)$ is the location of the substrate, $\hat{\mathbf{e}}_3$ is a unit vector normal to the substrate, and y is the perpendicular distance from \mathbf{r} to the substrate. The coordinates x^1 and x^2 are substrate coordinates used to localize points on the substrate. For example, in Section II B we will use the Monge parametrization, $\mathbf{X} = (x^1 \ x^2 \ f(x^1, x^2))^T$, where f gives the height of the substrate.

The tangent vectors to the substrate are

$$\mathbf{e}_\alpha = \partial_\alpha \mathbf{X} \quad (\text{II.2})$$

where $\partial_\alpha := \partial/\partial x^\alpha$. The coordinate vectors associated with the coordinate system are found from (II.1),

$$\tilde{\mathbf{e}}_\alpha = \partial_\alpha \mathbf{r} = \mathbf{e}_\alpha - y \mathbb{K}_\alpha^\beta \mathbf{e}_\beta, \quad \frac{\partial \mathbf{r}}{\partial y} = \hat{\mathbf{e}}_3, \quad (\text{II.3})$$

where we assume the summation of repeated indices, and Greek indices only take the value 1 or 2. We have also defined the curvature tensor \mathbb{K}_α^β from

$$\partial_\alpha \hat{\mathbf{e}}_3 = -\mathbb{K}_\alpha^\beta \mathbf{e}_\beta, \quad (\text{II.4})$$

since changes in the unit vector $\hat{\mathbf{e}}_3$ must be perpendicular to $\hat{\mathbf{e}}_3$, and $\hat{\mathbf{e}}_3 \cdot \mathbf{e}_\alpha = 0$. Note that the \mathbf{e}_α are not necessarily orthogonal or normalised.

We adopt the convention that quantities with a tilde are evaluated in the ‘bulk’ (away from the substrate), and thus depend on y , whilst those without the tilde are ‘substrate’ quantities and do not depend on y . Thus, $\tilde{\mathbf{e}}_\alpha(x^1, x^2, 0) = \mathbf{e}_\alpha(x^1, x^2)$. Starting in Section III, we will also denote quantities evaluated on the free surface at $y = \eta$ by an overbar.

The three-dimensional metric tensor $\tilde{\mathbf{g}}_{ab}$ has components

$$\tilde{\mathbf{g}}_{\alpha\beta} = \tilde{\mathbf{e}}_\alpha \cdot \tilde{\mathbf{e}}_\beta = \tilde{\mathbb{G}}_{\alpha\beta}, \quad \tilde{\mathbf{g}}_{\alpha 3} = \tilde{\mathbf{e}}_\alpha \cdot \hat{\mathbf{e}}_3 = 0, \quad \tilde{\mathbf{g}}_{33} = \hat{\mathbf{e}}_3 \cdot \hat{\mathbf{e}}_3 = 1,$$

where

$$\begin{aligned} \tilde{\mathbb{G}}_{\alpha\beta} &:= \tilde{\mathbf{e}}_\alpha \cdot \tilde{\mathbf{e}}_\beta = \mathbb{G}_{\alpha\beta} - 2y \mathbb{K}_{\alpha\beta} + \{y\}^2 \mathbb{K}_\alpha^\gamma \mathbb{K}_{\gamma\beta}, \\ \mathbb{G}_{\alpha\beta} &:= \mathbf{e}_\alpha \cdot \mathbf{e}_\beta, \end{aligned} \quad (\text{II.5})$$

and we have written the symmetric tensor $\mathbb{K}_{\alpha\beta} = \mathbb{K}_\alpha^\gamma \mathbb{G}_{\beta\gamma}$ in the usual manner of lowering indices with the metric tensor.^{14–16} The three-dimensional metric tensor is thus block-diagonal,

and the y coordinate is unstretched compared to the Cartesian coordinate system. It measures the true perpendicular distance from the substrate to a point in the fluid. Note that it is important that indices be raised or lowered with the appropriate metric: $\mathbb{G}_{\alpha\beta}$ for substrate quantities, $\tilde{\mathbf{g}}_{ab}$ or $\tilde{\mathbb{G}}_{\alpha\beta}$ for bulk quantities. The tensor $\tilde{\mathbb{G}}_{\alpha\beta}(x^1, x^2, y)$ can be used to raise or lower indices, even though it depends on three coordinates but only has two-dimensional indices, because of the block-diagonality of the metric $\tilde{\mathbf{g}}_{ab}$. Note also that in Eq. (II.5) we have written $\{y\}^2$ rather than y^2 , since the second form could be misinterpreted as the second contravariant component of y (which is nonsense in this case). We shall follow this practice throughout the paper, but note that negative powers are written as y^{-2} , since then there is no confusion.

Given the substrate vectors \mathbf{e}_α , it is easy to solve for the covectors \mathbf{e}^α , which are such that $\mathbf{e}^\alpha \cdot \mathbf{e}_\beta = \delta_\beta^\alpha$. Then the bulk covectors are

$$\tilde{\mathbf{e}}^\alpha = \mathbf{e}^\alpha + y \mathbb{K}_\beta^\alpha \mathbf{e}^\beta + \mathcal{O}(\{y\}^2), \quad (\text{II.6})$$

to first order in y , which can be checked by taking their dot product with the coordinate vectors (II.3) to see that $\tilde{\mathbf{e}}^\alpha \cdot \tilde{\mathbf{e}}_\beta = \delta_\beta^\alpha + \mathcal{O}(\{y\}^2)$. We will not need the covectors to higher order in y . From (II.6), we find the inverse metrics,

$$\begin{aligned} \tilde{\mathbb{G}}^{\alpha\beta} &= \tilde{\mathbf{e}}^\alpha \cdot \tilde{\mathbf{e}}^\beta = \mathbb{G}^{\alpha\beta} + 2y \mathbb{K}^{\alpha\beta} + \mathcal{O}(\{y\}^2), \\ \mathbb{G}^{\alpha\beta} &= \mathbf{e}^\alpha \cdot \mathbf{e}^\beta, \end{aligned} \quad (\text{II.7})$$

where again the higher-order terms will not be needed.

A crucial quantity is the determinant of the metric,

$$\tilde{w} = (\det \tilde{\mathbb{G}}_{\alpha\beta})^{1/2} = \tilde{\omega} w, \quad w = (\det \mathbb{G}_{\alpha\beta})^{1/2}, \quad (\text{II.8})$$

where

$$\tilde{\omega} = 1 - \kappa y + \mathcal{G} \{y\}^2, \quad (\text{II.9})$$

and

$$\kappa = \mathbb{K}_\alpha^\alpha \quad \text{mean curvature} \quad (\text{II.10a})$$

$$\mathcal{G} = \det \mathbb{K}_\alpha^\beta \quad \text{Gaussian curvature.} \quad (\text{II.10b})$$

The area element at fixed y is given by $\tilde{\omega} w dx^1 dx^2$, and the volume element by $\tilde{\omega} w dx^1 dx^2 dy$, since the y coordinate is unstretched with respect to the Cartesian system. The volume per unit substrate area of a fluid layer of thickness η is thus

$$\zeta = \frac{\int_0^\eta \tilde{\omega} w dx^1 dx^2 dy}{w dx^1 dx^2} = \eta - \frac{1}{2} \kappa \{\eta\}^2 + \frac{1}{3} \mathcal{G} \{\eta\}^3. \quad (\text{II.11})$$

The quantity $\tilde{\omega}$ also tells us when the coordinate system ceases to be valid: if $\tilde{\omega} = 0$, then the area element becomes singular. Hence, the valid range for y is

$$0 \leq y < \{\max(k_1, k_2, 0^+)\}^{-1}, \quad k_{1,2} := \frac{1}{2}(\kappa \pm \sqrt{\{\kappa\}^2 - 4\mathcal{G}})$$

where k_1 and k_2 are the principal curvatures.¹³ If both principal curvatures are negative then the positive range in y is unrestricted (convex region); otherwise y is limited by the largest positive principal curvature.

We now have all the geometrical equipment we need to solve fluid equations on the curved substrate. Note that all the results of this section are exact, except for the covectors (II.6) and inverse metric (II.7), which are valid to first order in y .

B. Substrate Coordinates

For most applications in the literature of thin films, orthonormal coordinates have been the coordinates of choice. This is because the main substrate shapes that have been treated are planes, cylinders, and spheres, where orthonormal coordinates are readily available. For a general substrate shape, orthonormal coordinates are difficult to construct and require numerical integration. Singularities (umbilics) also cause problems.¹³ For our application—flow down a curved substrate—the Monge representation of a surface¹⁷ is the most convenient.

The Monge representation is a glorified name for a parametrization of the substrate by

$$\mathbf{X}(x^1, x^2) = (x^1 \ x^2 \ f(x^1, x^2))^T \quad (\text{II.12})$$

in three-dimensional Cartesian space. Following standard notation,¹⁷ we define

$$p = \partial_1 f, \quad q = \partial_2 f, \quad (\text{II.13a})$$

$$r = \partial_1 \partial_1 f, \quad s = \partial_1 \partial_2 f, \quad t = \partial_2 \partial_2 f. \quad (\text{II.13b})$$

The unnormalized, nonorthogonal tangents \mathbf{e}_1 and \mathbf{e}_2 are

$$\mathbf{e}_1 = \partial_1 \mathbf{X} = (1 \ 0 \ p)^T, \quad \mathbf{e}_2 = \partial_2 \mathbf{X} = (0 \ 1 \ q)^T,$$

and their normalised cross product gives the normal to the substrate,

$$\hat{\mathbf{e}}_3 = \frac{1}{w} (-p \ -q \ 1)^T.$$

The corresponding covectors are

$$\mathbf{e}^1 = \frac{1}{\{w\}^2} ((1 + \{q\}^2) \ -pq \ p)^T, \quad \mathbf{e}^2 = \frac{1}{\{w\}^2} (-pq \ (1 + \{p\}^2) \ q)^T$$

and $\hat{\mathbf{e}}_3$ is its own covector. The metric tensor of the substrate and its inverse are

$$\{\mathbb{G}_{\alpha\beta}\} = \mathbf{e}_\alpha \cdot \mathbf{e}_\beta = \begin{pmatrix} 1 + \{p\}^2 & pq \\ pq & 1 + \{q\}^2 \end{pmatrix}, \quad \{\mathbb{G}^{\alpha\beta}\} = \mathbf{e}^\alpha \cdot \mathbf{e}^\beta = \frac{1}{\{w\}^2} \begin{pmatrix} 1 + \{q\}^2 & -pq \\ -pq & 1 + \{p\}^2 \end{pmatrix}, \quad (\text{II.14})$$

with determinant

$$w = (\det \mathbb{G}_{\alpha\beta})^{1/2} = \sqrt{1 + \{p\}^2 + \{q\}^2}.$$

The curvature tensor is

$$\{\mathbb{K}_\alpha{}^\beta\} := \frac{1}{\{w\}^3} \begin{pmatrix} (1 + \{q\}^2)r - pqs & (1 + \{p\}^2)s - pqr \\ (1 + \{q\}^2)s - pqt & (1 + \{p\}^2)t - pqs \end{pmatrix} \quad (\text{II.15})$$

which gives mean and Gaussian curvatures

$$\begin{aligned} \kappa &= \mathbb{K}_\alpha{}^\alpha = \frac{1}{\{w\}^3} ((1 + \{q\}^2)r - 2pqs + (1 + \{p\}^2)t), \\ \mathcal{G} &= \det \mathbb{K}_\alpha{}^\beta = \frac{1}{\{w\}^4} (rt - \{s\}^2). \end{aligned}$$

We write the normalized gravity vector as $\hat{\mathbf{g}} = (\sin \theta \cos \phi \ \sin \theta \sin \phi \ - \cos \theta)^T$, so that the inclination angle θ is zero for gravity pointing downwards, and for $\phi \in (-\pi/2, \pi/2)$ positive θ induces flow in the positive x^1 direction. Then we have the components

$$\begin{aligned}\hat{g}_s^1 &= \hat{\mathbf{g}} \cdot \mathbf{e}^1 = - (p \cos \theta + pq \sin \theta \sin \phi - (1 + \{q\}^2) \sin \theta \cos \phi) / \{w\}^2, \\ \hat{g}_s^2 &= \hat{\mathbf{g}} \cdot \mathbf{e}^2 = - (q \cos \theta + pq \sin \theta \cos \phi - (1 + \{p\}^2) \sin \theta \sin \phi) / \{w\}^2, \\ \hat{g}_y &= \hat{\mathbf{g}} \cdot \hat{\mathbf{e}}_3 = - (\cos \theta + p \sin \theta \cos \phi + q \sin \theta \sin \phi) / w.\end{aligned}\quad (\text{II.16})$$

The specific parametrization of the substrate introduced in this section will not be needed in the derivation of the equations of motion (Sections III and IV), only in their solution (Section V B). Hence, a different parametrization could be used if called for by the geometry of the substrate. For instance, flow down a curved filament is better parametrized by cylindrical coordinates, or if the substrate has overhangs (making f multivalued) coordinates based on arc length are better.

III. MASS CONSERVATION

We remind the reader of our notational convention:

1. Quantities with a **tilde** (e.g., $\tilde{\mathbf{e}}_\alpha$ and \tilde{w}) are evaluated between the substrate and the free surface (in the ‘bulk’) and are functions of (x^1, x^2, y, τ) .
2. Quantities with an **overbar** (e.g., $\bar{\mathbf{e}}_\alpha$ and \bar{w}) are evaluated on the free surface $y = \eta(x^1, x^2, \tau)$ and are functions of (x^1, x^2, τ) .
3. ‘Bare-headed’ quantities (e.g., \mathbf{e}_α and w) are evaluated on the substrate $y = 0$ and are functions of (x^1, x^2) , or they are quantities that do not depend on y at all (e.g., $\hat{\mathbf{e}}_3$).

We introduce a velocity field

$$\mathbf{u} = \tilde{u}^\alpha \tilde{\mathbf{e}}_\alpha + \tilde{v} \hat{\mathbf{e}}_3, \quad (\text{III.1})$$

associated with some time-dependent incompressible flow. Here we depart from RRS⁸ in two ways: first, the $\tilde{\mathbf{e}}_\alpha$ are not unit vectors, so the velocity components \tilde{u}^α are scaled differently; second, we use $\tilde{\mathbf{e}}_\alpha$ and not \mathbf{e}_α , so that the velocity field is expressed in terms of the bulk coordinate vectors rather than the substrate tangent vectors. This is slightly more natural in the present context, but is not crucial.

Mass conservation is imposed via the divergence-free condition, $\nabla \cdot \mathbf{u} = 0$; in terms of the coordinates in section II, this is

$$\partial_\alpha (\tilde{w} \tilde{u}^\alpha) + \frac{\partial}{\partial y} (\tilde{w} \tilde{v}) = 0. \quad (\text{III.2})$$

We integrate this from 0 to η and use the no-throughflow condition $\tilde{v}(x^1, x^2, 0) = 0$ to get

$$\bar{w} \bar{v} = - \int_0^\eta \partial_\alpha (\tilde{w} \tilde{u}^\alpha) \, dy \quad (\text{III.3})$$

$$= \bar{w} \bar{u}^\alpha \partial_\alpha \eta - \partial_\alpha \int_0^\eta (\tilde{w} \tilde{u}^\alpha) \, dy. \quad (\text{III.4})$$

Now we use the kinematic boundary condition at the top surface,

$$\partial_\tau \eta + \bar{u}^\alpha \partial_\alpha \eta = \bar{v}, \quad (\text{III.5})$$

to find

$$\bar{w} \partial_\tau \eta = -\partial_\alpha \int_0^\eta (\tilde{w} \tilde{u}^\alpha) \, dy. \quad (\text{III.6})$$

We define the mass flux vector

$$\tilde{q}^\alpha(x^1, x^2, y) := \int_0^y \tilde{\omega} \tilde{u}^\alpha dy, \quad \tilde{q}^\alpha(x^1, x^2) = \tilde{q}^\alpha(x^1, x^2, \eta) \quad (\text{III.7})$$

which allows us to rewrite (III.6) as

$$\bar{w} \partial_\tau \eta = -\partial_\alpha (w \tilde{q}^\alpha).$$

We divide through by w ,

$$\bar{\omega} \partial_\tau \eta = -\nabla_\alpha \tilde{q}^\alpha \quad (\text{III.8})$$

where the covariant divergence $\nabla_\alpha \tilde{q}^\alpha := w^{-1} \partial_\alpha (w \tilde{q}^\alpha)$, with ∇_α denoting the covariant derivative with respect to x^α using the substrate metric $\mathbb{G}_{\alpha\beta}$.¹⁴⁻¹⁶ In Eq. (III.8), $\tilde{\omega}$ defined by Eq. (II.9) is evaluated at $y = \eta$, and τ only enters $\tilde{\omega}$ through η . Hence, we can rewrite (III.8) as

$$\frac{\partial \zeta}{\partial \tau} + \nabla_\alpha \tilde{q}^\alpha = 0, \quad (\text{III.9})$$

where ζ is the volume per unit substrate area given by Eq. (II.11). Equation (III.9) thus embodies mass conservation.

Note that there were no assumptions on the thickness of the layer in this section.

IV. DYNAMICAL EQUATIONS OF MOTION

Sections III involved only kinematic considerations, namely mass conservation and the kinematic boundary conditions at the free surface and bottom substrate. Hence, everything we have done so far applies to any incompressible flow. Now we will restrict to the problem of a viscous (Stokes) flow driven by gravity, which satisfies the equation

$$\Delta \mathbf{u} = \nabla p - \hat{\mathbf{g}}, \quad (\text{IV.1})$$

where p is the pressure and $\hat{\mathbf{g}}$ is a unit vector in the direction of gravity. The velocity satisfies the boundary conditions

$$\mathbf{u} = 0 \quad \text{at } y = 0 \quad \text{no-slip at substrate} \quad (\text{IV.2a})$$

$$\mathbf{t}_\alpha \cdot \mathbb{T} \cdot \hat{\mathbf{n}} = 0 \quad \text{at } y = \eta \quad \text{tangential stresses at free surface} \quad (\text{IV.2b})$$

$$-p + \hat{\mathbf{n}} \cdot \mathbb{T} \cdot \hat{\mathbf{n}} = \sigma \kappa_{\text{surf}} \quad \text{at } y = \eta \quad \text{normal stress at free surface} \quad (\text{IV.2c})$$

$$\partial_\tau \eta + \bar{u}^\alpha \partial_\alpha \eta = \bar{v} \quad \text{at } y = \eta \quad \text{kinematic condition at free surface} \quad (\text{IV.2d})$$

where

$$\mathbb{T} := \nabla \mathbf{u} + (\nabla \mathbf{u})^T$$

is the deviatoric stress, $\hat{\mathbf{n}}$ is the unit normal to the surface, \mathbf{t}_α are tangents to the surface, and κ_{surf} is the mean curvature of the surface. The stress conditions assumes that the gas above the surface has negligible viscosity and density.

We have absorbed the constant density, viscosity, and strength of gravity into the velocity and pressure, so \mathbf{u} stands for $(\nu \mathbf{u}/g)$, p stands for $(p/g\rho)$, and the surface tension σ (introduced below) stands for $(\sigma/g\rho)$. This means that the velocity in (IV.1) has units of squared length, the pressure has units of length, and the surface tension has units of squared length.

In the coordinates of Section II, the location of the surface is

$$\bar{\mathbf{r}}(x^1, x^2, \tau) = \mathbf{X}(x^1, x^2) + \eta(x^1, x^2, \tau) \hat{\mathbf{e}}_3(x^1, x^2)$$

and the surface tangents $\bar{\mathbf{t}}_\alpha$ are then given by

$$\bar{\mathbf{t}}_\alpha = \partial_\alpha \bar{\mathbf{r}} = \bar{\mathbf{e}}_\alpha + \partial_\alpha \eta \hat{\mathbf{e}}_3. \quad (\text{IV.3})$$

The unit normal $\hat{\mathbf{n}}$ is obtained by taking the cross product of the tangents and normalizing.

In the coordinates introduced in Section II, with the velocity field (III.1), The Stokes Eq. (IV.1) becomes

$$\frac{1}{\tilde{w}} \left\{ \partial_\alpha \left(\tilde{w} \tilde{\mathbb{G}}^{\alpha\beta} \partial_\beta \right) + \frac{\partial}{\partial y} \left(\tilde{w} \frac{\partial}{\partial y} \right) \right\} (\tilde{u}^\gamma \tilde{\mathbf{e}}_\gamma + \tilde{v} \hat{\mathbf{e}}_3) = \tilde{\mathbf{e}}^\alpha \partial_\alpha p + \hat{\mathbf{e}}_3 \frac{\partial p}{\partial y} - \hat{g}_s^\alpha \mathbf{e}_\alpha - \hat{g}_y \hat{\mathbf{e}}_3, \quad (\text{IV.4})$$

where we wrote

$$\hat{\mathbf{g}} = \hat{g}_s^\alpha \mathbf{e}_\alpha + \hat{g}_y \hat{\mathbf{e}}_3$$

with components given by (II.16). Note that, unlike the velocity field (III.1), we have *not* written the gravity vector in terms of the bulk (tilde) coordinate vectors. This is to avoid y dependence in \hat{g}_s^α and \hat{g}_y .

A. Small-parameter Rescaling

Following RRS,⁸ we rescale the variables to account for the thinness of the fluid layer. We do this not by rescaling y , but by rescaling x^α : we treat the variations in the substrate as being large-scale, whilst the depth of the layer is of order unity. Hence, we introduce the rescalings

$$x^\alpha = \varepsilon^{-1} x^{\alpha*}, \quad \tilde{v} = \varepsilon \tilde{v}^*, \quad p = \varepsilon^{-1} p^*, \quad \sigma = \varepsilon^{-2} \sigma^*,$$

where ε is a small parameter; all other variables are left unscaled. Following standard practice, we immediately drop the $*$ superscripts and deal only with the rescaled variables. The amplitude of the variations of the substrate are taken to be such that the vectors \mathbf{e}_α and hence the substrate metric \mathbb{G} are of order unity. All terms involving the curvature tensor \mathbb{K} are of order ε , because of the $\partial/\partial x^\alpha$ in the definition (II.4).

The continuity equation (III.2) is unchanged by the rescalings, and neither is the kinematic boundary condition (III.5). The dynamical equation (IV.4) becomes

$$\frac{1}{\tilde{w}} \left\{ \{\varepsilon\}^2 \partial_\alpha \left(\tilde{w} \tilde{\mathbb{G}}^{\alpha\beta} \partial_\beta \right) + \frac{\partial}{\partial y} \left(\tilde{w} \frac{\partial}{\partial y} \right) \right\} (\tilde{u}^\gamma \tilde{\mathbf{e}}_\gamma + \varepsilon \tilde{v} \hat{\mathbf{e}}_3) = \tilde{\mathbf{e}}^\alpha \partial_\alpha p + \varepsilon^{-1} \hat{\mathbf{e}}_3 \frac{\partial p}{\partial y} - \hat{g}_s^\alpha \mathbf{e}_\alpha - \hat{g}_y \hat{\mathbf{e}}_3, \quad (\text{IV.5})$$

where $\tilde{w} = w(1 - \varepsilon \kappa y) + \mathcal{O}(\{\varepsilon\}^2)$, $\tilde{e}_\alpha = \mathbf{e}_\alpha - \varepsilon y \mathbb{K}_\alpha^\beta \mathbf{e}_\beta$, and $\tilde{e}^\alpha = \mathbf{e}^\alpha + \varepsilon y \mathbb{K}_{\alpha\beta} \mathbf{e}^\beta + \mathcal{O}(\{\varepsilon\}^2)$. As for the boundary conditions (IV.2), they simplify to

$$\tilde{u}^\alpha = \tilde{v} = 0 \quad \text{at } y = 0; \quad (\text{IV.6a})$$

$$\frac{\partial \tilde{u}^\alpha}{\partial y} = 0 + \mathcal{O}(\{\varepsilon\}^2) \quad \text{at } y = \eta; \quad (\text{IV.6b})$$

$$p = -\sigma \kappa_{\text{surf}} + \mathcal{O}(\{\varepsilon\}^2) \quad \text{at } y = \eta, \quad (\text{IV.6c})$$

where

$$\kappa_{\text{surf}} = \kappa + \varepsilon \eta \kappa_2 + \varepsilon \Delta \eta + \mathcal{O}(\{\varepsilon\}^2)$$

with $\Delta \eta = \nabla_\alpha \nabla^\alpha \eta = w^{-1} \partial_\alpha (w \mathbb{G}^{\alpha\beta} \partial_\beta \eta)$ the covariant Laplacian of η , and

$$\kappa_2 := \mathbb{K}_\alpha^\beta \mathbb{K}_\beta^\alpha.$$

We shall not need the higher-order terms in (IV.6).

B. Velocity Field

We now proceed in the usual manner and expand the fields as power series in ε :

$$\begin{aligned} \tilde{u}^\alpha &= \tilde{u}_{(0)}^\alpha + \varepsilon \tilde{u}_{(1)}^\alpha + \dots, \\ \tilde{p} &= \tilde{p}_{(0)} + \varepsilon \tilde{p}_{(1)} + \dots, \end{aligned}$$

where we have left out \tilde{v} since it is not needed in our development until later (and it will not appear as an asymptotic series). At order ε^0 , the velocity field and pressure satisfy

$$\frac{\partial^2 \tilde{u}_{(0)}^\alpha}{\partial \{y\}^2} = \partial^\alpha \tilde{p}_{(0)} - \hat{g}_s^\alpha, \quad \frac{\partial \tilde{p}_{(0)}}{\partial y} = 0,$$

where $\partial^\alpha = \mathbb{G}^{\alpha\beta} \partial_\beta$. These are readily integrated to give

$$\tilde{u}_{(0)}^\alpha = A_{(0)}^\alpha y(y - 2\eta), \quad \tilde{p}_{(0)} = -\sigma \kappa, \quad (\text{IV.7})$$

where

$$A_{(0)}^\alpha = -\frac{1}{2} (\hat{g}_s^\alpha + \sigma \partial^\alpha \kappa) \quad (\text{IV.8})$$

and the boundary conditions (IV.6) have been applied.

At order ε ,

$$\frac{\partial^2 \tilde{u}_{(1)}^\alpha}{\partial \{y\}^2} = (\kappa \delta_\beta^\alpha + 2 \mathbb{K}_\beta^\alpha) \frac{\partial \tilde{u}_{(0)}^\beta}{\partial y} + \partial^\alpha \tilde{p}_{(1)} + 2y \mathbb{K}_\beta^\alpha \partial^\beta \tilde{p}_{(0)} - y \hat{g}_s^\beta \mathbb{K}_\beta^\alpha, \quad \frac{\partial \tilde{p}_{(1)}}{\partial y} = \hat{g}_y,$$

with solution

$$\tilde{u}_{(1)}^\alpha = A_{(1)}^\alpha y(y - 2\eta) + B_{(1)}^\alpha y (\{y\}^2 - 3\{\eta\}^2) \quad (\text{IV.9})$$

where

$$A_{(1)}^\alpha = \frac{1}{2} (\hat{g}_s^\alpha \kappa \eta + 3\hat{g}_s^\beta \mathbb{K}_\beta^\alpha \eta - \hat{g}_y \partial^\alpha \eta + \sigma \{ \eta (\kappa \partial^\alpha \kappa + 2 \mathbb{K}_\beta^\alpha \partial^\beta \kappa) - \partial^\alpha (\kappa_2 \eta + \Delta \eta) \}), \quad (\text{IV.10a})$$

$$B_{(1)}^\alpha = -\frac{1}{6} (\hat{g}_s^\beta + \sigma \partial^\beta \kappa) (\kappa \delta_\beta^\alpha + 4 \mathbb{K}_\beta^\alpha). \quad (\text{IV.10b})$$

To simplify these expressions, we made use of

$$\partial_\alpha \hat{g}_y = \partial_\alpha (\hat{\mathbf{g}} \cdot \hat{\mathbf{e}}_3) = -\hat{\mathbf{g}} \cdot \mathbb{K}_\alpha^\beta \mathbf{e}_\beta = -\hat{g}_s^\beta \mathbb{K}_{\alpha\beta},$$

since $\hat{\mathbf{g}}$ is a constant vector.

Now that we have \tilde{u}^α to first order in ε , we can insert it in the definition of the mass flux vector (III.7),

$$\bar{q}^\alpha = \int_0^\eta \tilde{w} \tilde{u}^\alpha dy = \int_0^\eta (1 - \varepsilon \kappa y) (\tilde{u}_{(0)}^\alpha + \varepsilon \tilde{u}_{(1)}^\alpha) dy + \mathcal{O}(\{\varepsilon\}^2), \quad (\text{IV.11})$$

which gives

$$\bar{q}^\alpha = \bar{q}_{\text{grav}}^\alpha + \bar{q}_{\text{surf}}^\alpha \quad (\text{IV.12})$$

with

$$\begin{aligned} \bar{q}_{\text{grav}}^\alpha &= \frac{1}{3}\{\eta\}^3 \left\{ \hat{g}_s^\alpha - \varepsilon \hat{g}_s^\beta (\kappa \delta_\beta^\alpha + \frac{1}{2} \mathbb{K}_\beta^\alpha) \eta + \varepsilon \hat{g}_y \partial^\alpha \eta \right\} \\ &\quad + \{\varepsilon\}^2 \frac{1}{120} \{\eta\}^4 \kappa \left\{ \eta \hat{g}_s^\beta (9\kappa \delta_\beta^\alpha + 11 \mathbb{K}_\beta^\alpha) - 25 \hat{g}_y \partial^\alpha \eta \right\} + \mathcal{O}(\{\varepsilon\}^2), \end{aligned} \quad (\text{IV.13})$$

$$\begin{aligned} \bar{q}_{\text{surf}}^\alpha &= \frac{1}{3}\sigma\{\eta\}^3 \left\{ \partial^\alpha \kappa_{\text{surf}} - \varepsilon \eta \kappa \partial^\alpha \kappa + \frac{1}{2} \varepsilon \eta \mathbb{K}_\beta^\alpha \partial^\beta \kappa \right\} \\ &\quad + \{\varepsilon\}^2 \frac{1}{120} \sigma \{\eta\}^4 \kappa \left\{ 9\eta \kappa \partial^\alpha \kappa - 14 \eta \mathbb{K}_\beta^\alpha \partial^\beta \kappa - 25 \partial^\alpha (\kappa_2 \eta + \Delta \eta) \right\} + \mathcal{O}(\{\varepsilon\}^2), \end{aligned} \quad (\text{IV.14})$$

where we have kept some second-order terms but neglected others: this will be explained when we find \tilde{v} below and is related to the exact preservation of the kinematic constraints of the problem. Equation (III.9) with the flux (IV.12) is the dynamical equation that governs the evolution of η . To order ε , it is the same equation as that found by RRS,⁸ but in nonorthogonal coordinates rather than orthogonal coordinates. This is a straightforward generalization, but it is illuminating to rederive the equations in this setting, and allows a thorough introduction to all the notation. We will also need the quadratic terms in (IV.12) below, and these are not present in RRS's formulation: this is not a failure of RRS but rather is required by the specific application we have in mind, namely particle advection.

In order to do particle advection in Section VI, we will need the vertical velocity field, \tilde{v} . It is obtained by integrating the continuity equation (III.2),

$$\tilde{v} = -\frac{1}{\tilde{w}} \int_0^y \partial_\alpha (\tilde{w} \tilde{u}^\alpha) dy \quad (\text{IV.15})$$

where the integral's lower bound enforces the no throughflow boundary condition at $y = 0$. The kinematic boundary condition (III.5) is satisfied by (IV.15) at $y = \eta$, since

$$\begin{aligned} \bar{v} &= -\frac{1}{\bar{w}} \int_0^\eta \partial_\alpha (\tilde{w} \tilde{u}^\alpha) dy = -\frac{1}{\bar{w}} \partial_\alpha \int_0^\eta (\tilde{w} \tilde{u}^\alpha) dy + \frac{1}{\bar{w}} (\bar{w} \bar{u}^\alpha) \partial_\alpha \eta \\ &= -\frac{1}{\bar{w}} \partial_\alpha (\bar{w} \bar{q}^\alpha) + \bar{u}^\alpha \partial_\alpha \eta. \end{aligned} \quad (\text{IV.16})$$

The first term on the right-hand side of (IV.16) vanishes because of (III.9), and the second gives the kinematic boundary condition (III.5). But observe that to recover this boundary condition we need factors of \bar{w} to cancel; hence, a factor of \bar{w} must appear multiplicatively in the integrand if we are to satisfy the kinematic boundary condition *exactly* (*i.e.*, to all

orders in ε). This is the reason for keeping some second-order terms in (IV.11) and (IV.12). Note that this way the divergence-free condition (III.2) is also satisfied exactly.

The easiest way to get the y coefficients for v is to combine (IV.7) and (IV.9) into

$$\tilde{u}^\alpha = \tilde{u}_{(0)}^\alpha + \varepsilon \tilde{u}_{(1)}^\alpha = A^\alpha y (y - 2\eta) + B^\alpha y (\{y\}^2 - 3\{\eta\}^2), \quad (\text{IV.17})$$

valid to first order in ε , where $A^\alpha = A_{(0)}^\alpha + \varepsilon A_{(1)}^\alpha$ and $B^\alpha = \varepsilon B_{(1)}^\alpha$. Then, using $\tilde{w} = w(1 - \varepsilon\kappa y)$, we find from (IV.15)

$$\tilde{v} = \frac{\{y\}^2}{1 - \varepsilon\kappa y} (a + b y + c \{y\}^2 + d \{y\}^3) \quad (\text{IV.18})$$

where

$$\begin{aligned} a &= \frac{1}{2} \nabla_\alpha (2\eta A^\alpha + 3\{\eta\}^2 B^\alpha), & c &= \frac{1}{4} \nabla_\alpha (\varepsilon\kappa A^\alpha - B^\alpha), \\ b &= -\frac{1}{3} \nabla_\alpha ((1 + 2\varepsilon\kappa\eta) A^\alpha + 3\varepsilon\kappa\{\eta\}^2 B^\alpha), & d &= \frac{1}{5} \nabla_\alpha (\varepsilon\kappa B^\alpha), \end{aligned}$$

and the covariant divergence is defined after Eq. (III.8). The expression (IV.18) for \tilde{v} is exact, given the first-order expressions $\tilde{w} = w(1 - \varepsilon\kappa y)$ and (IV.17) for \tilde{u}^α .

V. SOLUTION OF THE EQUATIONS

We now seek steady solutions of Eq. (III.9) with the mass flux vector (IV.12). The unknown function is the thickness field $\eta(x^1, x^2)$. We characterize the shape of the substrate using the parametrization in Section II B, and assume the substrate is periodic in x^1 and x^2 with unit period. In dimensionless form, the independent input parameters of the problem are thus

1. The inclination angle θ and rotation angle ϕ of the gravity vector [Eq. (II.16)];
2. The thickness of the film at the corner, $\eta(0, 0) = \varepsilon$;
3. The shape of the substrate, including its height, specified with $f(x^1, x^2)$;
4. The surface tension σ .

The parameters 1 determines the speed and direction of the flow: the fluid is static for $\theta = 0$. Parameter 2, the thickness of the film at the corner, effectively determines ε . We shall thus drop ε from the equations for the remainder of the paper, instead introducing the small parameter through $\eta(0, 0) = \varepsilon$. Parameter 3 is infinitely rich: even for a given substrate shape, we can still vary its height by scaling f by a constant. We shall limit ourselves to substrates of relatively simple harmonic shapes.

A. Substrates with Translational Symmetry

Consider first the case where the substrate has a translational symmetry. We may then orient our coordinates such that f is only a function of x^2 . From Eq. (II.13), we then have $p = s = t = 0$. Since nothing depends on x^1 , we seek solutions of the form $\eta(x^2)$. Equation (III.9) then reduces to

$$\partial_2(w \bar{q}^2) = 0 \implies w \bar{q}^2 = \text{const.} \quad (\text{V.1})$$

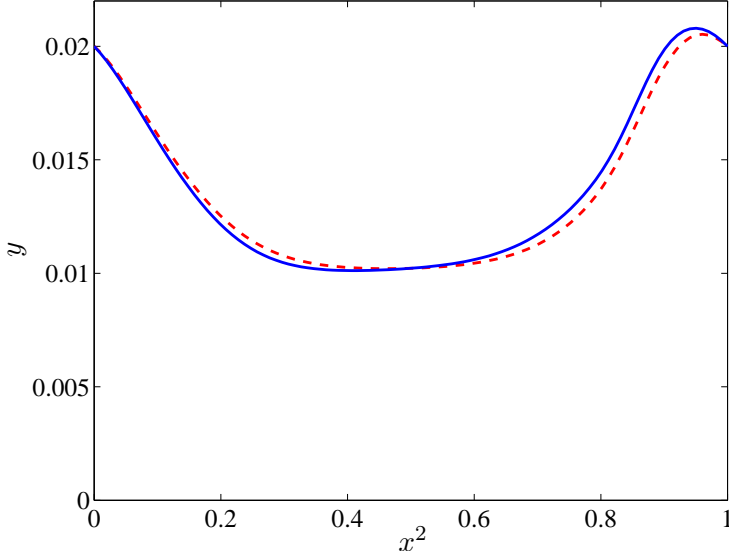


FIG. 1: Surface thickness $\eta(x^2)$ for a substrate with translational symmetry $f(x^2) = 0.1 \sin(2\pi x^2)$, for $\varepsilon = 0.02$, $\theta = 0.7$, $\phi = 1.2$, and $\sigma = 0$. The solid line is the zeroth-order analytic solution (V.2), and the dashed line is the first-order numerical solution.

since $\partial_1(\tilde{w}\bar{q}^1)$ vanishes. If we keep only the ε^0 terms in (IV.12), we can solve (V.1) analytically,

$$\eta(x^2) = (c w (\hat{g}_s^2 + \sigma w^{-2} \partial_2 \kappa))^{-1/3} \quad (\text{V.2})$$

where the constant c is adjusted to satisfy the boundary condition $\eta(0) = \varepsilon$, and we have used $\mathbb{G}^{22} = w^{-2}$. The quantity in parentheses in (V.2) can become singular or negative, an indication that the higher-order terms can no longer be neglected. In that case $\partial_2(w\bar{q}^2) = 0$ still holds but we then have to solve an ODE for $\eta(x^2)$. We shall not do this here and instead solve the general PDE in the next section. For comparison, the zeroth-order solution (V.2) is plotted along with the numerical first-order solution for a sinusoidal substrate and corner thickness $\varepsilon = 0.02$. The two agree well since the thickness is small.

Note that even though the velocity field depends only on two variables (x^2 and y), the flow is actually three-dimensional, since A^1 and B^1 in (IV.17) do not in general vanish, except in the special case $\phi = \pi/2$. We shall see in Section VI that even this simple solution supports rather complicated trajectories.

B. General Numerical Solution

In general, Eq. (III.9) with the mass flux vector (IV.12) must be solved numerically. We use a fourth-order finite-difference scheme together with Newton–Kantorovich iteration¹⁸ to converge to the steady solution. Since the N–K scheme employs a linearization of the nonlinear equation to seek an improved guess, it allows us to check the linear stability of the flow for free, and all the flows presented here are stable. In Figure 2 we show the thickness field of a typical solution, for the substrate

$$f(x^1, x^2) = 0.05 (\sin(2\pi x^1) \sin(2\pi x^2) + 0.2 \sin(4\pi x^2)) \quad (\text{V.3})$$

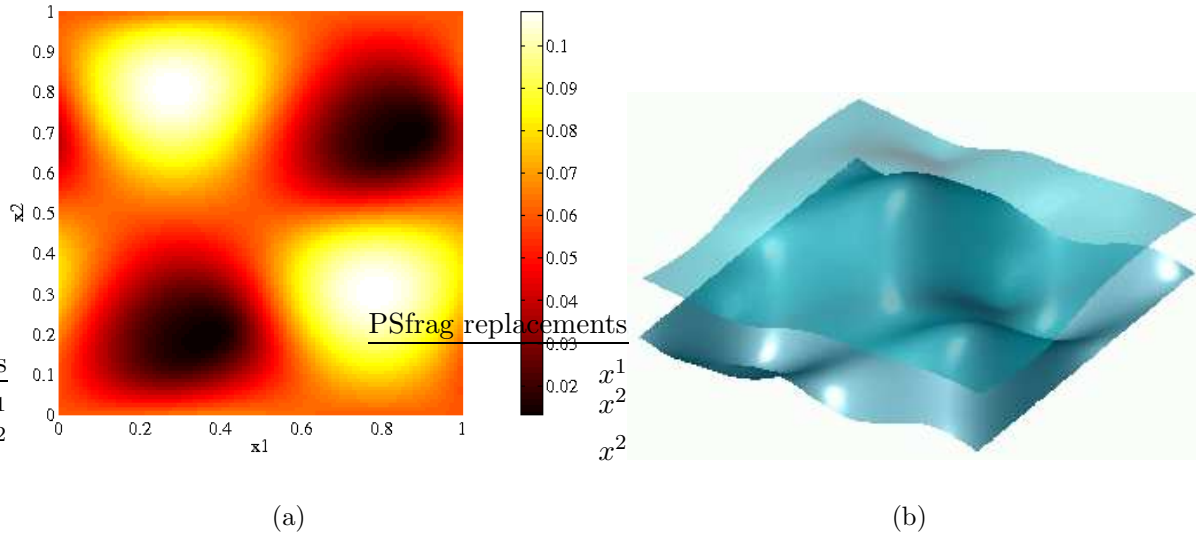


FIG. 2: The thickness field $\eta(x^1, x^2)$ for the substrate shape given by Eq. (V.3), with $\varepsilon = 0.06$, $\theta = 0.1$, $\phi = 0$, and $\sigma = 0$. (a) Contour plot: the flow is towards the right; (b) Surface plot: the flow is towards the upper-right. The vertical scale is exaggerated.

with $\varepsilon = 0.06$, $\theta = 0.1$, $\phi = 0$, and $\sigma = 0$. As mentioned in the introduction, we will set the surface tension to zero. The solutions presented in this paper typically have resolutions of 100×100 gridpoints, which is well-resolved enough. The acid test to see if we have enough numerical resolution is whether particle orbits ‘spiral in’ to attractors, which is precluded if the flow is incompressible. For example, the orbits in the regular islands of Fig. 5(a) are nice and closed over many periods.

When doing particle advection in Section VI the thickness field is first resampled on a grid of 1024×1024 using Fourier interpolation, and then the velocity field is evaluated off-gridpoints using linear interpolation. This has the advantage that the hardest part (the resampling) only needs to be done once at the beginning and stored. This is cheaper, for instance, than using a higher-order interpolation scheme on the coarser grid.

VI. FLUID PARTICLE TRAJECTORIES

To investigate the transport properties of the flow, we solve the advection equation

$$\partial_\tau \mathbf{r}(\tau) = \mathbf{u}(\mathbf{r}(\tau)), \quad \mathbf{r}(0) = \mathbf{r}_0, \quad (\text{VI.1})$$

for a steady velocity field \mathbf{u} of the form (III.1) obtained numerically as described in Section V. Instead of converting our velocity field back to Cartesian coordinates, we use the definition (II.1) of $\mathbf{r}(\tau)$ and take its time derivative, assuming that the coordinates are a function of time, and use the chain rule:

$$\partial_\tau \mathbf{r} = \partial_\alpha \mathbf{r} \partial_\tau x^\alpha + \partial_y \mathbf{r} \partial_\tau y = \partial_\tau x^\alpha \tilde{\mathbf{e}}_\alpha + \partial_\tau y \hat{\mathbf{e}}_3,$$

so that (VI.1) becomes

$$\partial_\tau x^\alpha = \tilde{u}^\alpha, \quad \partial_\tau y = \tilde{v}. \quad (\text{VI.2})$$

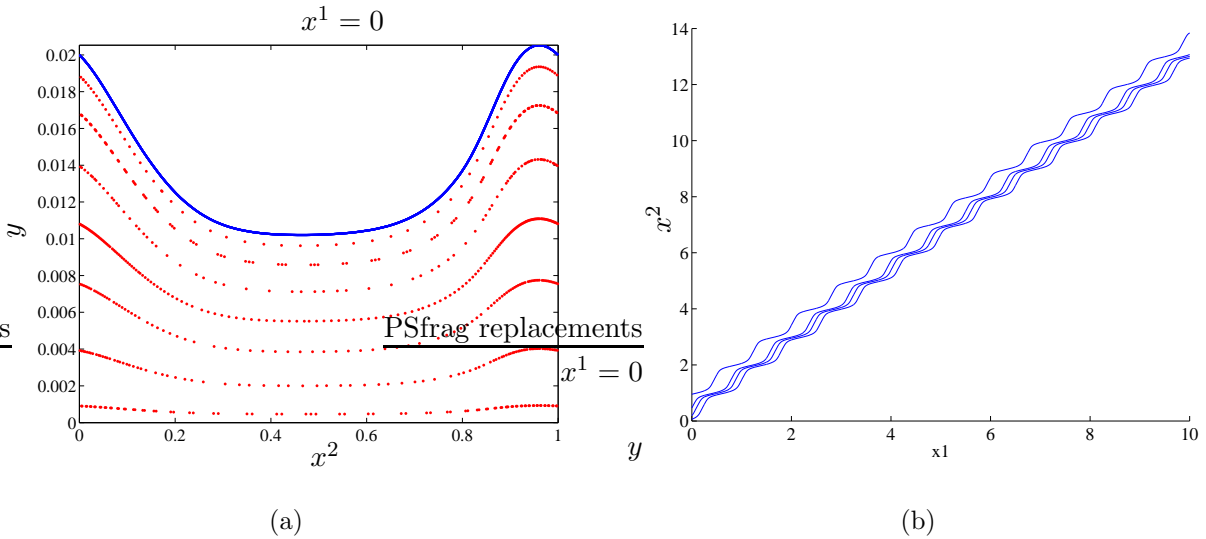


FIG. 3: For the same parameters as in Fig. 1: (a) Poincaré section at $x^1 = 0$; (b) Four typical trajectories at different depths y . The trajectories have the same overall slope.

We can thus follow particle trajectories in out curved coordinates using (VI.2). We will now do so for different types of substrates: those possessing translational symmetry (Section VI A) and those leading to chaotic trajectories (Section VI B). In all cases, the particle trajectories are computed using an adaptive embedded fourth/fifth-order Runge–Kutta scheme^{19,20} and the velocity field is interpolated as described in Section V B.

A. Substrates with Translational Symmetry

For substrates with translational symmetry, as described in Section V A, the system (VI.2) is

$$\partial_\tau x^1 = \tilde{u}^1(x^2, y), \quad \partial_\tau x^2 = \tilde{u}^2(x^2, y), \quad \partial_\tau y = \tilde{v}(x^2, y). \quad (\text{VI.3})$$

We may immediately write $x^1 = \tilde{u}^1(x^2, y) \tau + x_0^1$, so that (VI.3) is effectively an autonomous two-dimensional system, which is solvable by quadratures and cannot exhibit chaos.⁵ The system admits a streamfunction $\psi(x^2, y)$ such that

$$\tilde{u}^2 = \tilde{w}^{-1} \partial_y \psi, \quad \tilde{v} = -\tilde{w}^{-1} \partial_2 \psi$$

from which it is easily seen that $\psi = w \tilde{q}^2$, defined in (III.7). If the zeroth-order terms dominate everywhere, the resulting velocity profile is quadratic in y ('half-Poiseuille') and the flow in the x^2 - y plane cannot have a stagnation point inside the fluid, except at $y = 0$. Thus, a Poincaré section of trajectories, made by recording intersections with the plane $x^1 = 0$, must look like Fig. 3(a), where every trajectory crosses the domain in x^2 by going over furrows and crests. In Fig. 3(b) we see that four typical trajectories have roughly the same overall 'slope.' This leads to poor transport properties, since particles initially near each other remain near. This is due to the thinness of the layer which causes the zeroth-order velocity to dominate. If we use the zeroth order horizontal velocity (IV.7), we have

$$\tilde{u}_{(0)}^2 / \tilde{u}_{(0)}^1 = A_{(0)}^2 / A_{(0)}^1$$

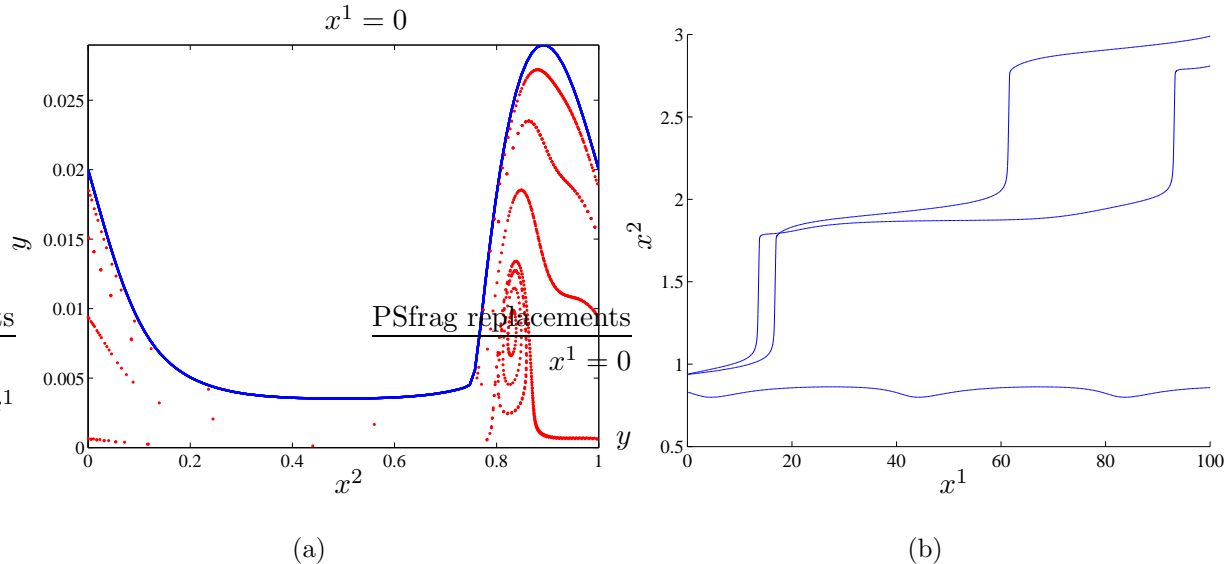


FIG. 4: For the same parameters as in Fig. 1 but with $\theta = 0.6$, $\phi = 0.8$: (a) Poincaré section at $x^1 = 0$, showing no apparent chaos; (b) The types of trajectories seen in (a): the bottom trajectory is trapped in a furrow, whilst the top two trajectories moves rapidly over crests, and more slowly over furrows. The three trajectories start at different depths y . Four typical trajectories, showing a trapped trajectory and three trajectories that undergo regular ‘near-trapping’ events. Note that the overall slopes of the trajectories are different, and are not monotonic with depth.

independent of the depth y . This implies that when the layer is very thin the trajectories in Fig. 3(b) are independent of depth. (This is true for any substrate, not just those with translational symmetry.) First-order corrections terms are required in order to have more complicated dynamics.

If the inclination angle θ of the substrate is decreased, or ϕ is changed so that the furrows present a more acute angle to the incoming flow, then a situation as in Fig. 4 develops. Here some of the fluid cannot make it over the crests and is trapped in a recirculating region. The trajectories that are not trapped go very quickly when over crests, as indicated by the paucity of points in the shallow regions of the Poincaré section Fig. 4(a), and linger over furrows, where the fluid is deeper. This is of course a consequence of mass conservation, as the fluid is forced to flow more rapidly in the shallows. Three representative trajectories are depicted in Figure 4(b), where the change in speed in the untrapped trajectory (top) is reflected in the slope of the curve. In contrast to Fig. 3(b), the overall slope of a trajectory now depends on its depth. This important effect, reflected in the different slopes of the trajectories in Fig. 4(b), leads to enhanced transport, in the sense that particles at different depths have very different histories. Furthermore, the slope (or lateral drift rate) of a trajectory is not monotonic in the depth, since it is due to a complicated resonance between the lateral motion and downslope topography.

If the inclination angle θ is too small, or ϕ is such that the furrows are too aligned with the incoming flow, then untrapped trajectories disappear but the flow also develops dry spots, since the fluid doesn’t make it over the crests of the bumps: it is flowing in the ‘gutters’ of the substrate. This takes us outside the scope of the present theory and we do not consider such cases.

B. Chaotic Trajectories

In Section VIA we looked at trajectories for the simplest type of substrate, those possessing a translational symmetry. We now want to investigate the potential for creating flows that exhibit chaotic trajectories, leading to chaotic advection.²⁻⁴ Breaking the translational symmetry of the substrate is essential for the existence of chaotic trajectories, otherwise the trajectories obey a two-dimensional autonomous system, as in Section VIA, which cannot exhibit chaos. Given that this translational symmetry is broken, there are three modifications to the flow that increase the chances of developing chaotic trajectories:

1. Break discrete symmetries of the substrate;
2. Make the fluid deeper (but still thin);
3. Make the inclination angle θ smaller.

The first point removes barriers to transport associated with symmetries.²¹⁻²⁵ The second point allows particles more vertical freedom to break the two-dimensional constraint that leads to integrable motion, by bringing in first-order terms in the velocity field. The third point allows the particles more time to move laterally during one periodic length of the domain by decreasing the flow velocity. Here, by laterally we mean a direction perpendicular to the mean flow.

As an illustration we will use the substrate with height function given by (V.3). The first term in (V.3) breaks the translational symmetry, and the second term is a perturbation that breaks the discrete symmetry $x^2 \rightarrow x^2 + \frac{1}{2}$. Thus, the substrate with those parameter values has a good chance of exhibiting chaos, according to our first point above.

Consider for an inclination angle $\theta = 0.2$ for the substrate (V.3), with a corner thickness $\varepsilon = 0.06$. This means that the fluid is reasonably thick, so our second point is satisfied. But the Poincaré section in Fig. 5(a) clearly shows that no chaos is present, since the phase space is foliated by one-dimensional curves. (Though very small regions of chaos could in principle be present, they are clearly not important here.) Figure 5(b) shows four typical trajectories, taken at about the same initial x^2 but at different depths y . The three untrapped trajectories undergo ‘near-trapping,’ in the sense that they appear to flirt with the idea of entering the trapped regions. This motion is periodic, but the period depends on the trajectory. There is thus a depth dependence as for the case in Fig. 4.

Now we apply our third modification from the list above and decrease the inclination angle to $\theta = 0.1$. This gives the thickness field depicted in Fig. 2. Figure 6(a) shows a Poincaré section for the resulting flow. The phase space clearly exhibits considerable chaotic behavior, as evidenced by the Poincaré section not being foliated by one-dimensional surfaces [compare to Fig. 5(a)]. There are still a few regions of regular behavior, indicated by the four visible islands, which correspond to islands in Fig. 5(a). In Figure 6(b) six trajectories are plotted: the bottom three are trapped in the islands. The top three undergo transitions between long untrapped motions, where the trajectories go diagonally across the substrate, and short trapped motions. This trapped-untrapped behavior is typical of chaotic dynamics in the neighborhood of islands.^{26,27}

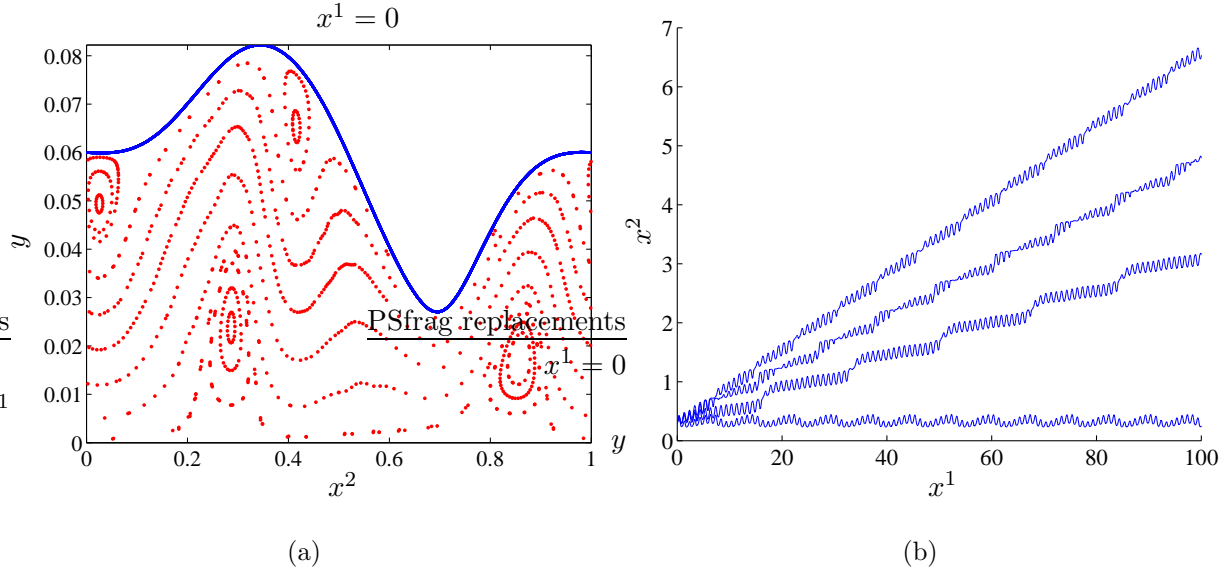


FIG. 5: For the substrate shape (V.3) with corner-thickness $\varepsilon = 0.06$ and inclination angle $\theta = 0.1$: (a) Poincaré section at $x^1 = 0$, showing no apparent chaos; (b) Four typical trajectories, showing a trapped trajectory and three trajectories that undergo regular ‘near-trapping’ events. Note that the overall slopes of the trajectories are different, and are not monotonic with depth.

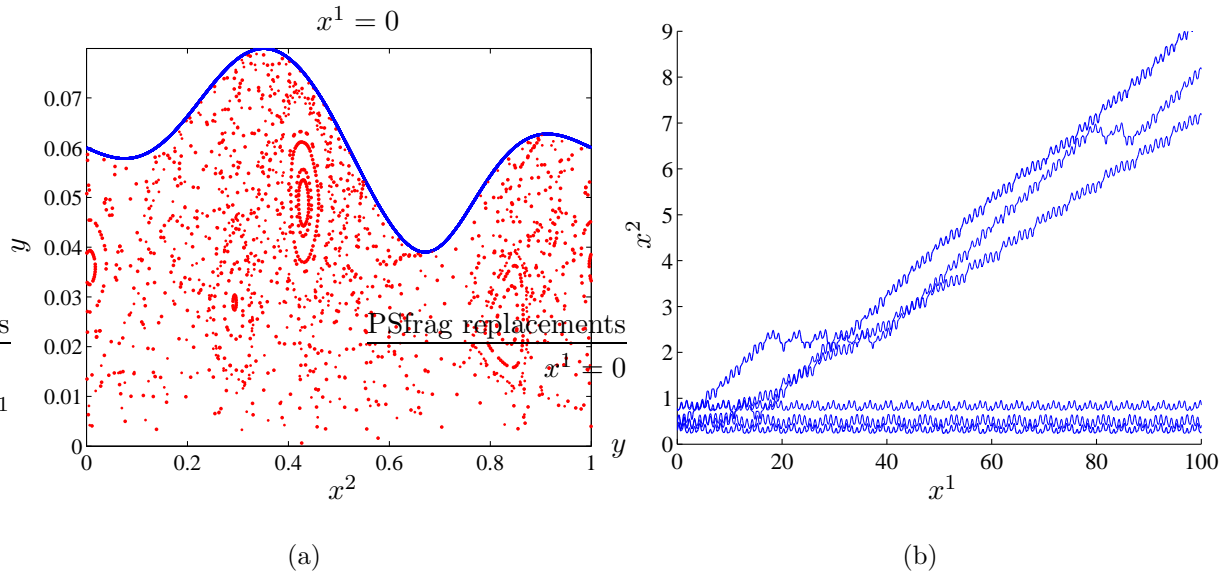


FIG. 6: For same parameters as the flow used for Fig. 5 but with a shallower inclination angle $\theta = 0.1$: (a) Poincaré section at $x^1 = 0$, showing considerable chaos; (b) Six typical trajectories, showing three trapped trajectories and three trajectories that undergo trapping events and flights typical of chaotic dynamics.

VII. DISCUSSION

We have derived an equation describing the gravity-driven motion of a thin viscous flow on a curved substrate. This is the same equation as in RRS⁸ expressed in nonorthogonal coordinates, and in addition including second-order correction terms to satisfy exactly the kinematic boundary condition at the free surface. This is essential for particle advection, since otherwise the small errors at the surface are enough to cause the particles to escape the domain.

We then investigated the character of fluid trajectories for four cases of increasing complexity. We observe a hierarchy of complex motions:

- For a substrate with translational symmetry at a large inclination angle, the flow is very thin and particle moves in uniform layers, as in Fig. 3(a). The lateral motion of the particles is essentially independent of their depth [Fig. 3(b)].
- For the same substrate with a smaller inclination angle, the flow becomes thicker over furrows, and zones of recirculation form. These are seen as islands in Fig. 4(a). Two new effects are visible in the particles trajectories [Fig. 4(b)]: some are trapped inside the rolls, and others exhibit different rates of lateral displacement in x^2 . This means that this flow has much better transport properties since particles initially near each other will separate rapidly (but not exponentially since there is no chaos).
- If we break the translational symmetry and use a fully two-dimensional surface such as (V.3), we observe the formation of more islands (four visible in total) of trapped trajectories [Fig. 5(a)]. The trajectories ‘bounce off’ the various islands causing complicated, but regular, oscillations [Fig. 5(b)].
- Finally, decreasing the inclination angle of the previous substrate preserves the same four islands [Fig. 6(a)], but now the trajectories undergo a succession of random trapped and untrapped events, analogous to Lévy flights observed in experiments in a rotating tank [Fig. 6(b)].^{26,27} This is the most effective transport achieved here, since particles initially near each other will separate exponentially, unless they are both inside the same island.

We used three modifications to the flow to increase the complexity of particle trajectories: 1. Breaking discrete symmetries of the substrate; 2. Making the fluid deeper; 3. Making the inclination angle smaller. Of the three, we expect the first two to have a similar effect on any other type of thin flow, say one driven by Marangoni stresses or shear at the free surface. The last simply says that decreasing the mean velocity of the flow can make lateral motions more important, heightening the chance of observing complex dynamics.

The lateral motion (that is, perpendicular to the mean flow direction) of particles is fairly small. We have made little effort to optimize this, preferring to focus our attention on test cases as a first object of study. Experiments would be desirable here to see if the observed lateral motion is of the right order of magnitude.

It is tempting to try to compute numerically an effective diffusion coefficient by simulating large numbers of particle trajectories. However, the numerical codes used here are too slow to achieve the high statistics needed to measure these coefficients with confidence. Rather, we hope to use techniques from homogenization theory to calculate the large-scale transport properties.²⁸

The generalized coordinate setting introduced in Section II is applicable to any set of dynamical equations, and could be used to model flows over complicated substrates in a fairly straightforward manner. It also allows for a time-dependent substrate, such as when it grows by solidification,⁹ though we have not treated such effects here.

Finally, the substrates used here were periodic in both directions, but it would be useful to quantify transport for random landscapes, consisting for instance of imperfections on the surface of a material.

Acknowledgments

We thank Richard Craster for his valuable advice. J-LT was funded in part by the UK Engineering and Physical Sciences Research Council grant GR/S72931/01.

1. A. Oron, S. H. Davis, and S. G. Bankoff, “Long-scale evolution of thin liquid films,” *Rev. Mod. Phys.* **63**, 931 (1997).
2. H. Aref, “Stirring by chaotic advection,” *J. Fluid Mech.* **143**, 1 (1984).
3. J. M. Ottino, *The Kinematics of Mixing: Stretching, Chaos, and Transport* (Cambridge University Press, Cambridge, U.K., 1989).
4. S. Wiggins and J. M. Ottino, “Foundations of chaotic mixing,” *Phil. Trans. R. Soc. Lond. A* **362**, 937 (2004).
5. J.-P. Eckmann and D. Ruelle, “Ergodic theory of chaos and strange attractors,” *Rev. Mod. Phys.* **57**, 617 (1985).
6. A. D. Stroock, S. K. W. Dertinger, A. Ajdari, I. Mezić, H. A. Stone, and G. M. Whitesides, “Chaotic mixer for microchannels,” *Science* **295**, 647 (2002).
7. M. P. Ida and M. J. Miksis, “The dynamics of thin films I: General theory,” *SIAM J. Appl. Math.* **58**, 456 (1998).
8. R. V. Roy, A. J. Roberts, and M. E. Simpson, “A lubrication model of coating flows over a curved substrate in space,” *J. Fluid Mech.* **454**, 235 (2002).
9. T. G. Myers, J. P. F. Charpin, and S. J. Chapman, “The flow and solidification of a thin fluid film on an arbitrary three-dimensional surface,” *Phys. Fluids* **14**, 2788 (2002).
10. S. Kalliadasis and G. M. Homsy, “Steady free-surface thin film flows over topography,” *Phys. Fluids* **12**, 1889 (2000).
11. S. Kalliadasis and G. M. Homsy, “Stability of free-surface thin-film flows over topography,” *J. Fluid Mech.* **448**, 387 (2001).
12. A. Mazouchi and G. M. Homsy, “Free surface Stokes flow over topography,” *Phys. Fluids* **13**, 2751 (2001).
13. I. Kreyszig, *Differential Geometry* (University of Toronto Press, Toronto, 1959).
14. R. M. Wald, *General Relativity* (University of Chicago Press, Chicago, 1984).
15. J. L. Synge and A. Schild, *Tensor Calculus* (Dover, New York, 1978).
16. B. Schutz, *Differential Geometry* (Cambridge University Press, Cambridge, U.K., 1980).
17. H. Flanders, *Differential Forms with Applications to the Physical Sciences* (Dover, New York, 1990).
18. J. P. Boyd, *Chebyshev and Fourier Spectral Methods*, 2nd ed. (Dover, New York, 2000).

19. J. R. Cash and A. H. Karp, “A variable order Runge–Kutta method for initial value problems with rapidly varying right-hand sides,” *ACM Trans. Math. Soft.* **16**, 201 (1990).
20. J. R. Dormand and P. J. Prince, “A family of embedded Runge–Kutta formulae,” *J. Comp. Appl. Math.* **6**, 19 (1980).
21. J. G. Franjione, C.-W. Leong, and J. M. Ottino, “Symmetries with chaos: A route to effective mixing,” *Phys. Fluids A* **1**, 1772 (1989).
22. J. G. Franjione and J. M. Ottino, “Symmetry concepts for the geometric analysis of mixing flows,” *Philosophical Transactions: Physical Sciences and Engineering* **338**, 301 (1992).
23. J. M. Ottino, F. J. Muzzio, M. Tjahjadi, J. G. Franjione, S. C. Jana, and H. A. Kusch, “Chaos, symmetry, and self-similarity: Exploiting order and disorder in mixing processes,” *Science* **257**, 754 (1992).
24. S. C. Jana, M. Tjahjadi, and J. M. Ottino, “Chaotic mixing of viscous fluids by periodic changes in geometry: Baffled cavity flow,” *Am. Inst. Chem. Eng. J.* **40**, 1769 (1994).
25. I. Mezić and S. Wiggins, “On the integrability and perturbation of three-dimensional fluid flows with symmetry,” *J. Nonlinear Sci.* **4**, 157 (1994).
26. T. H. Solomon, E. R. Weeks, and H. L. Swinney, “Observation of anomalous diffusion and Lévy flights in a two-dimensional rotating flow,” *Phys. Rev. Lett.* **71**, 3975 (1993).
27. T. H. Solomon, E. R. Weeks, and H. L. Swinney, “Chaotic advection in a two-dimensional flow: Lévy flights and anomalous diffusion,” *Physica D* **76**, 70 (1994).
28. A. J. Majda and P. R. Kramer, “Simplified models for turbulent diffusion: Theory, numerical modelling and physical phenomena,” *Physics Reports* **314**, 237 (1999).